Exact seismic velocities for TI media and extended Thomsen formulas for stronger anisotropies

James G. Berryman

ABSTRACT

I explore a different type of approximation to the exact anisotropic wave velocities as a function of incidence angle in transversely isotropic (TI) media. This formulation extends the Thomsen weak anisotropy approach to stronger deviations from isotropy without significantly affecting the simplicity of the equations. One easily recognized improvement is that the extreme value of the quasi-SV-wave speed $v_{sv}(\theta)$ is located near the correct incidence angle $\theta = \theta_{ex}$, rather than always being at the position $\theta = 45^o$, which universally holds for Thomsen's approximation — although $\theta_{ex} \equiv 45^o$ is actually never correct for *any* TI anisotropic medium. Also, the magnitudes of all the wave speeds are typically (although there may be some exceptions depending on the actual angular location of the extreme value) more closely approximated for all values of the incidence angle. Furthermore, the value of a special angle θ_m (which is close to the location of the extreme and also required by the new formulas) can be deduced from the same data that are normally used in the weak anisotropy data analysis. All the main technical results presented are independent of the physical source of the anisotropy. To illustrate the use of the results obtained, two examples are presented based on systems having vertical fractures. The first set of model fractures has their axes of symmetry randomly oriented in the horizontal plane. Such a system is then isotropic in the horizontal plane and, thus, exhibits vertical transverse isotropic (VTI) symmetry. The second set of fractures also has its axes of symmetry in the horizontal plane, but (it is assumed) these axes are aligned so that the system exhibits horizontal transverse isotropic (HTI) symmetry. Both types of systems, as well as any other TI medium (whether due to fractures or layering or other physical causes) are more accurately treated with the new wave speed formulation.

INTRODUCTION

Thomsen's weak anisotropy formulation (Thomsen, 1986) was originally designed for media having vertical transversely isotropic (VTI) symmetry, but clearly applies equally well to any other TI media (for example HTI) with only very minor technical changes related to how the orientation of the axis of symmetry is labelled in Cartesian coordinates. This formulation is also independent of the natural mechanism producing the anisotropy, whether it be due to layering, or horizontal fractures, or randomly

oriented vertical fractures, or some other source. So the method has wide applicability for use in exploration problems. However, when the approximate results of the Thomsen's original formulation are compared to known exact results for the same VTI media, it is easy to see that there are some deficiencies. In particular, for VTI media, the vertically polarized (SV) shear wave will always have a peak (or possibly a trough, for some fairly rare types of anisotropic media) somewhere in the range $0 \leq \theta \leq \pi/2 = 90^o$. Thomsen's weak anisotropy formulation always puts this extreme point (either minimum or maximum) exactly at $\theta = \pi/4 = 45^o$. However, as I show here, the $\theta = 45^o$ angular location never actually occurs for any interesting degree of VTI anisotropy; instead $\theta \to 45^o$ (by which I mean the extreme point approaches but never reaches 45^o) for extremely weak anisotropy — *e.g.*, very low horizontal crack density is one example of this. In an effort to determine whether it might be possible to improve on Thomsen's approximation, I have found that a relatively small modification of Thomsen's formulas places the extreme v_{sv} point at nearly the right angular location, and also typically (though not universally) improves the overall fit of both $v_{sv}(\theta)$ and $v_p(\theta)$ to the exact VTI curves. The ultimate cost of this improvement is negligible since the data required to estimate the location of the extreme point are exactly the same as the data used to determine Thomsen's other parameters for weak anisotropy. The method can also be used with only minor technical modifications for media having horizontal transversely isotropic (HTI) symmetry, such as reservoirs having aligned vertical fractures. The paper focuses on the general theory and uses other recent work relating fracture influence parameters (Sayers and Kachanov, 1991; Berryman and Grechka, 2006) to provide some useful examples of the applicability of the new method. Other choices of the various possible applications of the new method will appear in later publications.

The main result of the paper — from which all the subsequent results follow — is a new, more compact, and more intuitive way of writing the quantity $\zeta(\theta)$ [appearing here in equation 12]. This quantity has its extreme value at almost the same location as that of the quasi-SV-wave phase velocity, and this angular location is very easy to determine.

The following section reviews the standard results for wave speeds in a VTI medium, and also presents the Thomsen weak anisotropy results. The next section presents the analysis leading to the extended (*i.e.*, improving on Thomsen) anisotropy formulation, which allows the wave speed formulas to reflect more accurately the correct behavior near the extremes (greatest excursions from the values at normal incidence and near horizontal incidence). Then, the next section shows how to determine the value of θ_m (the incidence angle that determines where the extreme SV-wave behavior occurs) from the same data already used in Thomsen's formulas. Furthermore, normal moveout corrections are recomputed for the new formulation, and it is found that the results are identical to those for Thomsen formulation; thus, no new corrections are needed near normal incidence. Finally, to illustrate the results, models of VTI and HTI reservoirs having vertical fractures are computed using the new wave speed formulation and compared to prior results. Appendix A computes the quasi-SV-wave speed at $\theta = \theta_m$ exactly, and also at two levels of approximation

in order to have values to check against the corresponding results in the main text. Appendix B discusses how to get HTI results simply and directly from VTI results, both for the exact wave speeds and for the new approximate wave speed formulas. The final section of the main text presents an overview and suggests some possible applications of the results.

THOMSEN'S WEAK ANISOTROPY FORMULATION FOR SEISMIC WAVES

Thomsen's weak anisotropy formulation (Thomsen, 1986), being a collection of approximations designed specifically for use in velocity analysis for exploration geophysics, is clearly not exact. Approximations incorporated into the formulas become most apparent for angles θ greater than about 15^o from the vertical, especially for compressional and vertically polarized shear wave velocities $v_p(\theta)$ and $v_{sv}(\theta)$, respectively. For VTI media, angle θ is measured from the $\hat{z}$-vector pointing directly into the earth.

For reference purposes, I include here the exact velocity formulas for; quasi-P, quasi-SV, and SH seismic waves at all angles in a VTI elastic medium. These results are available in many places (Postma, 1955; Musgrave, 1959, 2003; Rüger, 2002; Thomsen, 2002), but were taken directly from Berryman (1979) with only some minor changes of notation; specifically, the a,b,c,f,l,m notation for stiffnesses has been translated to the Voigt c_{ij} stiffness notation wherein $a \rightarrow c_{11}$, $b \rightarrow c_{12}$, $c \rightarrow c_{33}$, $f \rightarrow c_{13}$, $l \rightarrow c_{44}$, and $m \rightarrow c_{66}$. The results are:

$$v_p^2(\theta) = \frac{1}{2\rho}\left\{\left[(c_{11}+c_{44})\sin^2\theta + (c_{33}+c_{44})\cos^2\theta\right] + R(\theta)\right\} \tag{1}$$

and

$$v_{sv}^2(\theta) = \frac{1}{2\rho}\left\{\left[(c_{11}+c_{44})\sin^2\theta + (c_{33}+c_{44})\cos^2\theta\right] - R(\theta)\right\}, \tag{2}$$

where

$$R(\theta) = \sqrt{\left[(c_{11}-c_{44})\sin^2\theta - (c_{33}-c_{44})\cos^2\theta\right]^2 + 4\left(c_{13}+c_{44}\right)^2\sin^2\theta\cos^2\theta} \tag{3}$$

and, finally,

$$v_{sh}^2(\theta) = \frac{1}{\rho}\left[c_{44} + (c_{66}-c_{44})\sin^2\theta\right]. \tag{4}$$

I have purposely written equations 1 and 2 in this way to emphasize the fact that $v_p^2(\theta)$ and $v_{sv}^2(\theta)$ are closely related since they are actually the two solutions of a quadratic equation having the form:

$$\left(v^2\right)^2 - \left(v_p^2 + v_{sv}^2\right)v^2 + v_p^2 v_{sv}^2 = 0. \tag{5}$$

Any approximations made to one of these two wave speeds should therefore always be reflected in the other for this reason. In particular, any approximation to the square root in R should be made consistently for both v_p and v_{sv}.

For VTI symmetry, the stiffness matrix c_{ij} is defined for $i, j = 1, \ldots, 6$ by

$$c_{ij} = \begin{pmatrix} c_{11} & c_{12} & c_{13} & & & \\ c_{12} & c_{11} & c_{13} & & & \\ c_{13} & c_{13} & c_{33} & & & \\ & & & c_{44} & & \\ & & & & c_{44} & \\ & & & & & c_{66} \end{pmatrix}, \tag{6}$$

where $c_{12} = c_{11} - 2c_{66}$. In an isotropic system (which is a more restrictive case than our current interests), $c_{12} = c_{13} = \lambda$, $c_{44} = c_{66} = \mu$, and $c_{11} = c_{33} = \lambda + 2\mu$, where λ and μ are the usual Lamé constants. The definition in equation 6 makes use of the Voigt notation, *i.e.,* 6×6 matrix instead of 4th order tensor, wherein Voigt single indices $i, j = 1, 2, 3, 4, 5, 6$ correspond to the pairs of tensor indices 11,22,33,23,31,12, respectively. And it relates stress σ_{ij} to strain ϵ_{ij} via $\sigma_{23} = c_{44}\epsilon_{23}$, $\sigma_{31} = c_{44}\epsilon_{31}$, $\sigma_{12} = c_{66}\epsilon_{12}$, and $\sigma_{ii} = \Sigma_j c_{ij}\epsilon_{jj}$ (no summation over repeated indices is assumed here) for $i, j = 1, 2, 3$. For VTI symmetry, we typically take $x_3 = z$ (the vertical) as the axis of symmetry. But, for HTI symmetry, we may choose index direction x_3 to be some other physical direction (such as horizontal directions x or y, or some linear combination thereof); having done this, equations 2–4 apply strictly only in the vertical plane perpendicular to the fracture plane, while a small amount of vector analysis is then required to obtain the velocity values at all azimuthal angles $\phi \neq \pi/2$ away from the fracture plane.

Expressions for phase velocities in Thomsen's weak anisotropy limit can be found in many places, including Thomsen (1986, 2002) and Rüger (2002). The pertinent expressions for phase velocities in VTI media as a function of angle θ, measured as previously mentioned from the vertical direction, are

$$v_p(\theta) \simeq v_p(0) \left(1 + \epsilon \sin^2\theta - (\epsilon - \delta) \sin^2\theta \cos^2\theta\right), \tag{7}$$

$$v_{sv}(\theta) \simeq v_s(0) \left(1 + \left[v_p^2(0)/v_s^2(0)\right] (\epsilon - \delta) \sin^2\theta \cos^2\theta\right), \tag{8}$$

and

$$v_{sh}(\theta) \simeq v_s(0) \left(1 + \gamma \sin^2\theta\right). \tag{9}$$

In our present context, $v_s(0) = \sqrt{c_{44}/\rho_0}$, and $v_p(0) = \sqrt{c_{33}/\rho_0}$, where c_{33}, c_{44}, and ρ_0 are two stiffnesses of the cracked medium and the mass density of the isotropic host elastic medium. [For the specific physical examples that follow involving models of fractured reservoirs, I assume that the cracks contain insufficient volume to affect the overall mass density significantly.] The three Thomsen (1986) seismic parameters appearing in equations 7–9 for weak anisotropy with VTI symmetry are $\gamma = (c_{66} - c_{44})/2c_{44}$, $\epsilon = (c_{11} - c_{33})/2c_{33}$, and

$$\delta = \frac{(c_{13} + c_{44})^2 - (c_{33} - c_{44})^2}{2c_{33}(c_{33} - c_{44})} = \left(\frac{c_{33} + c_{13}}{2c_{33}}\right)\left(\frac{c_{13} + 2c_{44} - c_{33}}{c_{33} - c_{44}}\right). \tag{10}$$

Parameter γ is a measure of the shear wave anisotropy and birefringence. Parameter ϵ is a measure of the quasi-P wave anisotropy. Parameter δ controls the complexity of the shape of the wave fronts for quasi-P and quasi-SV waves; *e.g.*, when $\delta = \epsilon$ the wave fronts are elliptical in shape, whereas for all TI anisotropic systems having $\epsilon - \delta \neq 0$, the wave front will deviate from being elliptical, and it is in such cases that ray arrival triplications may occur.

All three of these parameters γ, ϵ, δ can play important roles in the velocities given by equations 7–9 when the anisotropy is large, as would be the case in fractured reservoirs when the crack densities are high enough. If crack densities are very low, then the SV shear wave will actually have no dependence on angle of wave propagation. Note that the so-called anellipticity parameter (Dellinger *et al.*, 1993; Fomel, 2004; Tsvankin, 2005, p. 253), $A = \epsilon - \delta$, vanishes when $\epsilon \equiv \delta$ — which (as will be shown) does happen to a very good approximation for low crack densities. Then, the results are anisotropic but have the special (elliptical) shape to the wave front mentioned previously.

For each of these phase velocities, the derivation of Thomsen's approximation has included a step that removes the square on the left-hand side of equations 1, 2, and 4 — obtained by expanding a square root of the right hand side. This step introduces a factor of $\frac{1}{2}$ multiplying the $\sin^2\theta$ terms on the right hand side, and — for example — immediately explains how equation 8 is obtained from equation 4. The other two equations for $v_p(\theta)$ and $v_{sv}(\theta)$, *i.e.*, equations 7 and 8, involve additional approximations. More of the details about the nature of these approximations are elucidated by first obtaining an alternative approximate formulation.

EXTENDED APPROXIMATIONS FOR ANISOTROPIC WAVE SPEEDS

The biggest and most obvious problem with Thomsen's approximations to the wave speeds generally occurs in $v_{sv}(\theta)$. The key issue is that Thomsen's approximation for $v_{sv}(\theta)$ is completely symmetric around $\theta = \pi/4 = 45^o$, while unfortunately this is generally not true of the actual wave speeds $v_{sv}(\theta)$. This error may seem innocuous in itself since it is not immediately clear whether it affects the results for small angles of incidence ($< 15^o$) or not, but it can in fact lead to large over- or under-estimates of wave speeds in the neighborhood of both the extreme value located at $\theta = \theta_{ex}$ and also at $\theta = 45^o \neq \theta_{ex}$. To improve this situation while still making use of a practical approximation to the wave speed, I reconsider an approach originally proposed in Berryman (1979). In particular, notice that the square root formula for $R(\theta)$ can be conveniently, and exactly, rewritten as:

$$R(\theta) = [(c_{11} - c_{44})\sin^2\theta + (c_{33} - c_{44})\cos^2\theta]\sqrt{1 - \zeta(\theta)}, \tag{11}$$

where

$$\zeta(\theta) \equiv 4\frac{[(c_{11} - c_{44})(c_{33} - c_{44}) - (c_{13} + c_{44})^2]\sin^2\theta\cos^2\theta}{[(c_{11} - c_{44})\sin^2\theta + (c_{33} - c_{44})\cos^2\theta]^2}. \tag{12}$$

To simplify this expression, first notice that ζ has an absolute maximum value, which occurs when θ takes the value θ_m determined by

$$\tan^2\theta_m = \frac{c_{33}-c_{44}}{c_{11}-c_{44}}. \tag{13}$$

The extreme value of ζ is given by

$$\zeta_m = 1 - \frac{(c_{13}+c_{44})^2}{(c_{11}-c_{44})(c_{33}-c_{44})} = \frac{2(\epsilon-\delta)c_{33}}{c_{11}-c_{44}} = \frac{2(\epsilon-\delta)v_p^2(0)}{v_p^2(0)(1+2\epsilon)-v_s^2(0)}, \tag{14}$$

where the second and third expressions relate ζ_m to the difference between the Thomsen parameters ϵ and δ, and to $v_p(0)$ and $v_s(0)$. Then, $\zeta(\theta)$ can be rewritten as

$$\zeta(\theta) = \frac{2\zeta_m}{1+\chi(\theta)}, \tag{15}$$

where

$$\chi(\theta) = \frac{1}{2}\left[\frac{\tan^2\theta}{\tan^2\theta_m} + \frac{\tan^2\theta_m}{\tan^2\theta}\right]. \tag{16}$$

For realistic systems, it is always true that $\zeta(\theta) \le 1$. [For example, in the fractured reservoir examples presented later in the paper, the largest observed value of $\zeta_m \simeq 0.29$. Also, note $\zeta_m \ge 0$ for all layered media since $\epsilon - \delta \ge 0$ for layered elastic media (Postma, 1955; Backus, 1962; Berryman, 1979).] So, we can expand the square root in equation 11, keeping only its first order Taylor series correction, which is

$$\sqrt{1-\zeta(\theta)} \simeq 1 - \frac{\zeta(\theta)}{2} = 1 - \frac{\zeta_m}{1+\chi(\theta)}. \tag{17}$$

Results for $v_p(\theta)$ and $v_{sv}(\theta)$ then become:

$$v_p^2(\theta) \simeq \frac{1}{\rho}\left\{\left[c_{11}\sin^2\theta + c_{33}\cos^2\theta\right] - \frac{\zeta_m[(c_{11}-c_{44})\sin^2\theta + (c_{33}-c_{44})\cos^2\theta]}{2[1+\chi(\theta)]}\right\} \tag{18}$$

and

$$v_{sv}^2(\theta) \simeq \frac{1}{\rho}\left\{c_{44} + \frac{\zeta_m[(c_{11}-c_{44})\sin^2\theta + (c_{33}-c_{44})\cos^2\theta]}{2[1+\chi(\theta)]}\right\}. \tag{19}$$

Note that the only approximation made in arriving at equations 18 and 19 again was the approximation of the square root via equation 17.

Clearly, the analysis is not really restricted in any way to using just the first order Taylor approximation in equation 17. For example, other authors (Fowler, 2003; Pederson *et al.*, 2007) have explored rational approximations to such square roots at length. These approaches can certainly be useful in many applications as they provide higher order approximations (not necessarily just first and second order Taylor contributions), while avoiding the computational complexity of the square root operation. Nevertheless, such efforts are beyond our current scope and so will not be discussed further here.

Compact form for $\zeta(\theta)$

More progress can be made by first noting that the quantity $\frac{1}{2}[1+\chi(\theta)]$ may be written as a perfect square:

$$\frac{1}{2}[1+\chi(\theta)] = \frac{1}{4}\left(\frac{\tan\theta}{\tan\theta_m} + \frac{\tan\theta_m}{\tan\theta}\right)^2 = \frac{(\tan^2\theta + \tan^2\theta_m)^2}{4\tan^2\theta\tan^2\theta_m}. \tag{20}$$

This expression may be simplified using trigonometric identities in the following way. First multiply both the numerator and denominator of equation 20 by $\cos^4\theta\cos^4\theta_m$. The denominator of the result is then proportional to $\sin^2 2\theta \sin^2 2\theta_m$, which is a useful form that I will keep. The numerator however is now proportional to the square of

$$\cos^2\theta\cos^2\theta_m(\tan^2\theta+\tan^2\theta_m) = \sin^2\theta\cos^2\theta_m+\sin^2\theta_m\cos^2\theta = \frac{1}{2}\left(1-\cos 2\theta\cos 2\theta_m\right), \tag{21}$$

which is another useful form I want to keep. Combining equations 20 and 21, the final result for $\zeta(\theta)$ is therefore

$$\zeta(\theta) = \frac{\zeta_m \sin^2 2\theta_m \sin^2 2\theta}{\left[1-\cos 2\theta_m\cos 2\theta\right]^2}. \tag{22}$$

Equation 22 is the main technical result of this paper, and it is exact. No approximations were made in arriving at equation 22. [Remark: The only approximations made to the wave speeds anywhere in this paper involve Taylor expansions of square roots. So the first approximations made here, of the form $\sqrt{1-\zeta(\theta)} \simeq 1-\zeta(\theta)/2$, do not depend directly on a weak anisotropy assumption, but only on the smallness of ζ_m compared to unity. However, the second ones, *i.e.*, those removing the squares in the formulas for the velocities, do depend directly on a type of weak anisotropy assumption — similar in spirit to Thomsen's (1986) approximations.]

Combining equation 22 with definition 12, it can also be shown that

$$\begin{aligned}
\left[(c_{11}-c_{44})\sin^2\theta + (c_{33}-c_{44})\cos^2\theta\right]^2 &= (c_{11}-c_{44})(c_{33}-c_{44})\frac{4\zeta_m\sin^2\theta\cos^2\theta}{\zeta(\theta)} \\
&= (c_{11}-c_{44})(c_{33}-c_{44})\frac{\left[1-\cos 2\theta_m\cos 2\theta\right]^2}{\sin^2 2\theta_m} \\
&= (c_{11}-c_{44})^2\tan^2\theta_m\frac{\left[1-\cos 2\theta_m\cos 2\theta\right]^2}{4\sin^2\theta_m\cos^2\theta_m} \\
&= (c_{11}-c_{44})^2\frac{\left[1-\cos 2\theta_m\cos 2\theta\right]^2}{4\cos^4\theta_m}.
\end{aligned}$$

So it follows that

$$\sin^2\theta + \tan^2\theta_m\cos^2\theta = \frac{\left[1-\cos 2\theta_m\cos 2\theta\right]}{2\cos^2\theta_m}, \tag{23}$$

which is another useful identity that can be checked directly.

Then, making use of the identity $\sin^2 2\theta_m / \cos^2 \theta_m = 4 \sin^2 \theta_m$, the speed of the quasi-SV-wave is given by

$$\rho v_{sv}^2(\theta) \simeq c_{44} + (c_{11} - c_{44})\zeta_m \frac{2 \sin^2 \theta_m \sin^2 \theta \cos^2 \theta}{[1 - \cos 2\theta_m \cos 2\theta]}. \tag{24}$$

Similarly, the speed of the quasi-P-wave is given (also consistent with equation 24) by

$$\rho v_p^2 \simeq c_{33} + (c_{11} - c_{33}) \sin^2 \theta - (c_{11} - c_{44})\zeta_m \frac{2 \sin^2 \theta_m \sin^2 \theta \cos^2 \theta}{[1 - \cos 2\theta_m \cos 2\theta]}. \tag{25}$$

Again, the only approximation made in these two expressions is the one due to expanding the square root in equation 17.

A tedious but straightforward calculation based on equations 2, 11, and 23 shows that the extreme value of $v_{sv}(\theta)$ — although not exactly at $\theta = \theta_m$ — nevertheless occurs very close to this angle. This calculation is however more technical than others presented here, so it will not be shown explicitly, but the results are confirmed later in the graphical examples. A similar result (but not identical) holds for the extended Thomsen formulas that follow.

Extended Thomsen formulas

A more direct comparison with Thomsen's approximations uses equations 24 and 25 to arrive at approximate formulas for $v_{sv}(\theta)$ and $v_p(\theta)$ analogous to Thomsen's. The resulting expressions, which may be called "extended Thomsen formulas," are given by

$$v_p(\theta)/v_p(0) \simeq 1 + \epsilon \sin^2 \theta - (\epsilon - \delta) \frac{2 \sin^2 \theta_m \sin^2 \theta \cos^2 \theta}{[1 - \cos 2\theta_m \cos 2\theta]} \tag{26}$$

and

$$v_{sv}(\theta)/v_s(0) \simeq 1 + \left[v_p^2(0)/v_s^2(0)\right] (\epsilon - \delta) \frac{2 \sin^2 \theta_m \sin^2 \theta \cos^2 \theta}{[1 - \cos 2\theta_m \cos 2\theta]}. \tag{27}$$

Equations 26 and 27 are the two main *approximate* results of this paper. So far only two approximations have been made, and both of these came from expanding a square root in a Taylor series, and retaining only the first nontrivial term.

Comparing equations 26 and 27 to equations 6 and 7, the differences are found to lie in a factor of the form:

$$\frac{2 \sin^2 \theta_m}{[1 - \cos 2\theta_m \cos 2\theta]} \rightarrow \frac{1}{2 \cos^2 \theta_m} \qquad \text{as} \qquad \theta \rightarrow \theta_m, \tag{28}$$

which depends explicitly on the angle θ_m determined by $\tan^2 \theta_m = (c_{33} - c_{44})/(c_{11} - c_{44})$, and also on θ itself. As indicated, the expression goes to $1/2 \cos^2 \theta_m$ in the limit of $\theta \rightarrow \theta_m$, which is also in agreement with the results for $v_{sv}(\theta_m)$ in Appendix A.

But, since $\sin^2\theta_m = \tan^2\theta_m/(1+\tan^2\theta_m)$ and $\cos 2\theta_m = (1-\tan^2\theta_m)/(1+\tan^2\theta_m)$, useful identities are

$$\sin^2\theta_m = \frac{c_{33}-c_{44}}{c_{11}+c_{33}-2c_{44}} = 1-\cos^2\theta_m \tag{29}$$

and

$$\cos 2\theta_m = \frac{c_{11}-c_{33}}{c_{11}+c_{33}-2c_{44}} = 1-2\sin^2\theta_m. \tag{30}$$

These results can therefore be used, after deducing some of the elastic constants from field data at near offsets, in order to extend the validity of the equations to greater angles and farther offsets. Inversion of such data is however beyond this paper's scope.

To make the formulas 26 and 27 look as much as possible like Thomsen's formulas — and thereby arrive at a somewhat different understanding of equations 7 and 8, first eliminate θ_m by arbitrarily setting it equal to some value such as $\theta_m = 45^o$, in which case $2\sin^2\theta_m = 1$ and $\cos 2\theta_m = 0$. Then, the θ dependence in the denominators goes away, and Thomsen's formulas 7 and 8 are recovered exactly. The particular choice $\theta_m = 45^o$ is however completely unnecessary as shall be shown, and furthermore is never valid for any anisotropic medium having $c_{11} \neq c_{33}$.

DEDUCING θ_M FROM SEISMIC DATA

In the extended formulas for seismic data, the key quantity needed is clearly the value of the angle θ_m. However, this value is quite easily determined since

$$\tan^2\theta_m = \frac{c_{33}-c_{44}}{c_{11}-c_{44}} = \frac{v_p^2(0)-v_s^2(0)}{(c_{11}/\rho)-v_s^2(0)} \tag{31}$$

and

$$\epsilon = \frac{c_{11}-c_{33}}{2c_{33}} = \frac{c_{11}/\rho - v_p^2(0)}{2v_p^2(0)}. \tag{32}$$

Therefore,

$$\tan^2\theta_m = \frac{v_p^2(0)-v_s^2(0)}{(1+2\epsilon)v_p^2(0)-v_s^2(0)}. \tag{33}$$

Thus, θ_m is completely determined by the same data used in the standard analysis of reflection seismic data, which determines the various small angle wave speeds and the Thomsen weak anisotropy parameters.

The pertinent fixed factors for use in the formulas are given by

$$\sin^2\theta_m = \frac{v_p^2(0)-v_s^2(0)}{2[(1+\epsilon)v_p^2(0)-v_s^2(0)]} \tag{34}$$

and

$$\cos 2\theta_m = \frac{\epsilon v_p^2(0)}{(1+\epsilon)v_p^2(0)-v_s^2(0)}. \tag{35}$$

Finally, equation 14 also shows how to determine the extreme value $\zeta_m = \zeta(\theta_m)$ using the same data. Examples of such computations are presented in TABLE 1 for various anisotropic rock types. Data for these examples comes from Thomsen's TABLE 1, and no other information is required.

TABLE 1. Examples of ζ_m — *i.e.*, the extreme value $\zeta(\theta_m)$ — and its angular location θ_m for various rocks and minerals. The data for ϵ, δ, $v_p(0)$, and $v_s(0)$ are all taken from Table 1 of Thomsen (1986).

Sample	ϵ	δ	$v_p(0)$ (m/s)	$v_s(0)$ (m/s)	ζ_m	θ_m
Cotton Valley shale	0.135	0.205	4721.	2890.	-0.1564	39.89^o
Mesaverde sandstone	0.081	0.057	3688.	2774.	0.0805	40.48^o
Muscovite crystal	1.12	-0.235	4420.	2091.	0.8985	26.90^o
Pierre shale	0.015	0.060	2202.	969.	-0.1076	44.48^o
Taylor sandstone	0.110	-0.035	3368.	1829.	0.3135	41.12^o
Wills Point shale	0.215	0.315	1058.	387.	-0.1543	39.27^o

NORMAL MOVEOUT CORRECTIONS

The altered forms of $v_p(\theta)$ and $v_{sv}(\theta)$ in equations 26 and 27 suggest that it might also be necessary to alter the normal moveout (NMO) corrections to the velocities (Tsvankin, 2005, p. 113). It is easy to see that these corrections are now given by

$$V_{NMO,p} = v_p(0)\sqrt{1+2\delta}, \tag{36}$$

for the quasi-P-wave, and,

$$V_{NMO,sv} = v_s(0)\sqrt{1+2\sigma}, \tag{37}$$

for the quasi-SV-wave, where

$$\sigma = \left[v_p^2(0)/v_s^2(0)\right](\epsilon - \delta). \tag{38}$$

These corrections to the NMO velocities are exactly the same as those for Thomsen's weak anisotropy approximation because the factor that is pertinent, and that might have potential to alter these expressions is given, in the small angle limit $\theta \to 0$, by

$$\frac{2\sin^2\theta_m}{1-\cos 2\theta_m} \equiv 1, \tag{39}$$

which holds for any value of θ_m (including both $\theta_m \to 0$ and $\theta_m = 45^0$). Since Thomsen's formulas accurately approximate all three wave speeds in this limit by design, the present formulas share this accuracy (and in some cases — *i.e.*, larger offsets — improves upon it). Therefore, no changes are needed in short offset (small θ) data processing.

The NMO correction for the SH-wave clearly does not change either, since it does not depend on this new factor.

RESERVOIRS WITH VERTICALLY ORIENTED FRACTURES

To provide some pertinent examples of results for the types of anisotropic media most interesting in oil and gas reservoirs, two distinct types of reservoirs having vertical fractures will now be considered. The first case studied will have vertical fractures that are not preferentially aligned, so the reservoir symmetry is vertical transverse isotropy (VTI). The second case will also have vertical fractures but these will be preferentially aligned, so the reservoir symmetry will be horizontal transverse isotropy (HTI) and, therefore, exhibit azimuthal (angle ϕ dependent) anisotropy.

These two reservoir fracture models will be built up using results from recent numerical experiments by Grechka and Kachanov (2006a,b). Those results were analyzed by Berryman and Grechka (2006) in light of the crack influence parameter formalism of Kachanov (1980) and Sayers and Kachanov (1991). The significance of two crack influence parameters — η_i, for $i = 1, 2$ — for the case of aligned horizontal cracks for lower crack densities $\rho_c = na^3$ (where $n = N/V$ is the number density of cracks — N being the total number per volume V — and for penny-shaped cracks a is the radius of the circular penny crack-face while b/a is called the aspect ratio) is:

$$\Delta S_{ij}^{(1H)} = \rho_c \begin{pmatrix} 0 & 0 & \eta_1 & & & \\ 0 & 0 & \eta_1 & & & \\ \eta_1 & \eta_1 & 2(\eta_1+\eta_2) & & & \\ & & & 2\eta_2 & & \\ & & & & 2\eta_2 & \\ & & & & & 0 \end{pmatrix}. \tag{40}$$

For smaller values of crack density ρ_c, equation 40 shows how the presence of penny-shaped cracks increases the compliance of the reservoir. [Note that η_1 is usually small and most often negligible, while η_2 is positive and nonnegligible.] Typical values of crack density ρ_c for reservoirs are $\rho_c \leq 0.1$. The matrix $\Delta S_{ij}^{(1H)}$ is the lowest order compliance correction matrix and should be added to the isotropic compliance matrix

$$\Delta S_{ij}^{(0)} = \begin{pmatrix} 1/E & -\nu/E & -\nu/E & & & \\ -\nu/E & 1/E & -\nu/E & & & \\ -\nu/E & -\nu/E & 1/E & & & \\ & & & 1/G & & \\ & & & & 1/G & \\ & & & & & 1/G \end{pmatrix}, \tag{41}$$

where $\nu = \lambda/2(\lambda+\mu)$ is Poisson's ratio, $G = \mu$ is the shear modulus, and $E = 2(1+\nu)G$ is Young's modulus of the (assumed) isotropic background medium. Summing equations 41 and 40 produces the compliance matrix for a horizontally cracked, VTI elastic medium. This combined matrix is then used to compute the behavior of a

simple HTI reservoir with aligned vertical cracks using the methods described in Appendix B.

For vertical fractures with randomly oriented axes of symmetry, the resulting VTI medium has a low crack density correction matrix of the form

$$\Delta S_{ij}^{(1V)} = \rho_c \begin{pmatrix} (\eta_1+\eta_2) & \eta_1 & \eta_1/2 & & & \\ \eta_1 & (\eta_1+\eta_2) & \eta_1/2 & & & \\ \eta_1/2 & \eta_1/2 & 0 & & & \\ & & & \eta_2 & & \\ & & & & \eta_2 & \\ & & & & & 2\eta_2 \end{pmatrix}, \tag{42}$$

in which the η's have the same values as those in equation 40 if the only difference between the cracks in equations 42 and 40 is their orientation. Note that $2\Delta S_{ij}^{(1V)} + \Delta S_{ij}^{(1H)}$ is an isotropic correction matrix for a system having crack density $3\rho_c$. Summing equations 41 and 42 produces the compliance matrix for a vertically cracked VTI elastic medium, in which the crack normals are randomly and/or uniformly distributed in the horizontal plane.

Higher order corrections (*i.e.*, second order in powers of ρ_c) in the Sayers and Kachanov (1991) formulation with the three crack influence parameters η_i, for $i = 3, 4, 5$, take the form (again using the Voigt matrix notation):

$$\Delta S_{ij}^{(2H)} = \rho_c^2 \begin{pmatrix} 0 & 0 & \eta_4 & & & \\ 0 & 0 & \eta_4 & & & \\ \eta_4 & \eta_4 & 2(\eta_3+\eta_4+\eta_5) & & & \\ & & & 2\eta_5 & & \\ & & & & 2\eta_5 & \\ & & & & & 0 \end{pmatrix} \tag{43}$$

for horizontal fractures — *i.e.*, to be combined with equation 40. Similarly,

$$\Delta S_{ij}^{(2V)} = \rho_c^2 \begin{pmatrix} (\eta_3+\eta_4+\eta_5) & \eta_4 & \eta_4/2 & & & \\ \eta_4 & (\eta_3+\eta_4+\eta_5) & \eta_4/2 & & & \\ \eta_4/2 & \eta_4/2 & 0 & & & \\ & & & \eta_5 & & \\ & & & & \eta_5 & \\ & & & & & 2(\eta_3+\eta_5) \end{pmatrix} \tag{44}$$

for the random vertical fractures producing VTI symmetry – to be combined with equation 42.

Examples of values of all five of these crack influence parameters have been obtained based on the numerical studies of Grechka and Kachanov (2006a,b) by Berryman and Grechka (2006). The two models considered have very different Poisson's

ratios for the isotropic background media: (a) $\nu_0 = 0.00$ and (b) $\nu_0 = 0.4375$. We will call these two models, respectively, the first model and the second model. The first model has background stiffness matrix values $c_{11} = c_{22} = c_{33} = 13.75$ GPa, $c_{12} = c_{13} = c_{23} = 0.00$ GPa, and $c_{44} = c_{55} = c_{66} = 6.875$ GPa. Bulk modulus for this model is therefore $K_0 = 4.583$ GPa and shear modulus is $G_0 = 6.875$ GPa. The purpose of this model is to provide as much contrast as possible with the following model, while still retaining a physically pertinent value of Poisson's ratio (for which values typically lie in the range $0.0 \leq \nu_0 \leq 0.5$). The second model has stiffness matrix values $c_{11} = c_{22} = c_{33} = 19.80$ GPa, $c_{12} = c_{13} = c_{23} = 15.40$ GPa, and $c_{44} = c_{55} = c_{66} = 2.20$ GPa. Bulk modulus for this model is therefore $K_0 = 16.86$ GPa and shear modulus is $G_0 = 2.20$ GPa. The second model may be seen to correspond to a background material having compressional wave speed $V_p = 3$ km/s, shear wave speed $V_s = 1$ km/s, and mass density $\rho_m = 2200.0$ kg/m^3, and is therefore more typical of a sandstone reservoir. Detailed discussion of the method used to obtain the crack influence parameters is given by Berryman and Grechka (2006), and will not be repeated here. Results are listed in TABLE 2.

In all the following plots, the exact curves (as computed for the model c_{ij}'s) are plotted first in black; then the Thomsen approximation is plotted in red; and finally the new approximation is plotted in blue. Thus, in those examples where red curves appear to be missing, this happens because the blue curves lie right on top of the red ones (to graphical accuracy). This overlay effect is expected whenever θ_m approaches 45^o, which can happen at low crack densities since the background medium has been taken to be isotropic.

TABLE 2. Values of five fracture-influence parameters for the two models considered, from Berryman and Grechka (2006).

Fracture-influence Parameters	*First Model* $\nu_0 = 0.00$	*Second Model* $\nu_0 = 0.4375$
η_1 (GPa^{-1})	0.0000	-0.0192
η_2 (GPa^{-1})	0.1941	0.3994
η_3 (GPa^{-1})	-0.3666	-1.3750
η_4 (GPa^{-1})	0.0000	0.0000
η_5 (GPa^{-1})	0.0917	0.5500

TABLE 3. Values of ζ_m [the extreme value of $\zeta(\theta)$] for the four models considered. The model fracture density is ρ_c. The model Poisson ratio for the background medium is ν_0.

	ζ_m	ζ_m	ζ_m
Model	for $\rho_c = 0.05$	for $\rho_c = 0.10$	for $\rho_c = 0.20$
HTI, $\nu_0 = 0.00$	0.0277	0.0973	0.2943
VTI, $\nu_0 = 0.00$	0.0148	0.0558	0.1965
HTI, $\nu_0 = 0.4375$	0.0102	0.0441	0.1595
	for $\rho_c = 0.025$	for $\rho_c = 0.050$	for $\rho_c = 0.100$
VTI, $\nu_0 = 0.4375$	0.0011	0.0051	0.0210

For reference purposes, the computed values of ζ_m are also presented in TABLE 3.

VTI Symmetry

Figures 1–6 present results for the case of vertical fractures having an isotropic distribution of normals (symmetry axes) in the horizontal plane. The resulting medium has VTI symmetry.

A first observation is that the low crack density results for $v_{sv}(\theta)$ are nearly constant, showing that $\epsilon - \delta \simeq 0$. When this happens for $v_{sv}(\theta)$, it is also true that $v_p(\theta)$ is approximately elliptical. Of course, the exact results for $v_{sh}(\theta)$ are always elliptical, but the Thomsen and new approximate results are only approximately elliptical.

Secondly, all three velocity models (exact, Thomsen, and the new approximation) give very similar results for all cases shown when $\nu_0 = 0.4375$. There are however some significant differences among the results for $\nu_0 = 0.00$, especially for $v_{sv}(\theta)$ and $v_p(\theta)$ – the largest deviations from the exact curves being those for Thomsen's approximations (red curves) in both cases.

HTI Symmetry

Figures 7–12 present results for vertical fractures having their normals (axes of symmetry) aligned in some direction (say $x_3 = x$). The fracture models considered are the same and use the same data as for the preceding (VTI) case.

Thomsen's approximation and the new one are virtually identical here in $v_{sh}(\theta)$ for both $\nu_0 = 0.00$ and $\nu_0 = 0.4375$. For $v_{sv}(\theta)$, Thomsen's approximation is higher than the exact result, while the new approximation is lower.

Results for $v_p(\theta)$ in both Thomsen's and the new approximation are comparable to the exact results for θ's up to about 45^o–50^o, but are not identical to each other or to the exact result. For $\nu_0 = 0.4375$, agreement among the three curves is good for $v_p(\theta)$, but not so good for $v_{sv}(\theta)$ or $v_{sh}(\theta)$.

SUMMARY AND CONCLUSIONS

The main technical result of the paper is equation 22, showing directly how $\zeta(\theta)$ is related to θ_m and ζ_m. The most significant applications of this result are summarized in equations 26 and 27. These formulas generalize (*i.e.*, extend the validity of) Thomsen's weak anisotropy approach to wider ranges of angles, and stronger anisotropies. These formulas have the clear advantage that they require no more data analysis than Thomsen's formulas for weak anisotropy, but they give more accurate predictions of the wave speeds for longer offsets. In particular, the new formulas are designed to give the peak (or possibly the trough — if the difference $\epsilon - \delta$ happens to be negative) of the quasi-SV-wave in the right location, (*i.e.*, the correct angle $\theta = \theta_m$ with the vertical), even though the magnitude of these velocities may still be a bit off. For quasi-SV waves, this error made in the velocity magnitude is always less than that made using the original Thomsen formulas. For quasi-P waves the results are somewhat mixed because the errors introduced by poor approximations to $\zeta(\theta)$ can have either sign, positive or negative, depending on what the actual value of θ_m happens to be. This fact shows that Thomsen's approximation will sometimes give better results at smaller θ than the new formulas, but other times they will be worse. This fluctuation in the behavior for quasi-P waves is observed in the examples contained in the Figures. Thus, the new approximation does have the advantage of consistency.

Furthermore, the only new parameter needed for implementation is the angle θ_m itself; however, the value θ_m is also determined directly from the same data required to compute all the Thomsen parameters (for example, see TABLE 1). A final advantage that is especially helpful for the practical use of the method is that the corrections needed for all the NMO velocities do not change, and so are exactly the same as for Thomsen's formulation.

DISCUSSION

The work presented here has necessarily been restricted to VTI and HTI symmetries, because these correspond to the simplest and most studied cases in the anisotropy literature. It has sometimes been noted, however, that the HTI symmetry in particular is actually a fairly unrealistic model for seismic exploration problems (Schoenberg and Helbig, 1997; Tsvankin, 1997, 2005; Thomsen, 2002). The reason for this is that the earth, to a first approximation, is often horizontally layered and such horizontal layering is well-known to produce VTI symmetry (Postma, 1955; Backus, 1962). If aligned vertical fractures are superimposed on this already anisotropic background medium (unlike the isotropic background medium used in the models presented here), then the resulting symmetry is likely to be closer to orthorhombic (having nine independent elastic constants) than to HTI (having at most only five independent constants). This viewpoint no doubt provides a valid criticism of the work presented in the examples as far its value for practical applications. However, the author expects the present paper to be followed by others on this topic, and future efforts will be devoted to ob-

taining comparable results for such orthotropic systems (Mensch and Rasolofosaon, 1997), and thereby becoming more realistic for exploration purposes.

All the results presented here are specifically for phase velocities of the seismic waves. In heterogeneous media, it is instead the ray (or group) velocities that are needed for ray tracing applications, and in particular for wave equation migration. However, recent work by Zhu *et al.* (2005; 2007) has reformulated the Gaussian beam migration approach to permit direct use of phase velocities, with a corresponding reduction in the overall computational burden. Although it is too soon to be certain which potential applications of the results contained herein may prove to be of value, it is seems likely that this particular application will be one of the more interesting ones for seismic data analysis.

ACKNOWLEDGMENTS

The author thanks V. Grechka, M. Kachanov, S. Nakagawa, and I. Tsvankin for helpful discussions and suggestions.

APPENDIX A: $V_{SV}(\theta_M)$

For purposes of comparison, it is useful to know the exact value and also some related approximations to the exact value of the quasi-SV wave speed $v_{sv}(\theta)$ at the angle $\theta = \theta_m =$ — which occurs close to (but not exactly at) the extreme value of $v_{sv}(\theta)$ over all angles (see discussion after equation 25 in the main text).

Evaluation gives the exact result

$$v_{sv}^2(\theta_m) = \frac{\sin^2\theta_m}{2\rho}(c_{11}-c_{44})\left[\frac{c_{11}+c_{44}}{c_{11}-c_{44}} + \frac{c_{33}+c_{44}}{c_{33}-c_{44}} - 2\sqrt{1-\zeta_m}\right]. \tag{A-1}$$

After substituting $\sin^2\theta_m = (c_{33}-c_{44})/(c_{11}+c_{33}-2c_{44})$, expanding the square root $\sqrt{1-\zeta_m} \simeq 1-\zeta_m/2$, and several more steps of simplification, a useful approximate expression is

$$v_{sv}^2(\theta_m) \simeq v_s^2(0)\left[1 + \frac{\zeta_m}{2}\frac{(c_{11}-c_{44})(c_{33}-c_{44})}{c_{44}(c_{11}+c_{33}-2c_{44})}\right]. \tag{A-2}$$

And finally, by approximating the square root of this expression and using (14), we have

$$\frac{v_{sv}(\theta_m)}{v_s(0)} \simeq 1 + \frac{\zeta_m(c_{11}-c_{44})\sin^2\theta_m}{4c_{44}} = 1 + \left[v_p^2(0)/v_s^2(0)\right](\epsilon-\delta)\frac{\sin^2\theta_m}{2}. \tag{A-3}$$

Equation A-3 can be directly compared to Thomsen's formula for $v_{sv}(\theta)$ in equation 8. The only difference is a factor of $2\cos^2\theta_m$ in the final term. This factor could be unity if $\theta_m = 45^o$, but — since this never happens for anisotropic media — the factor always differs from unity and can be either higher or lower than unity depending on whether θ_m is less than or greater than 45^o.

APPENDIX B: HTI FORMULAS FROM VTI FORMULAS

Probably the easiest way to obtain formulas pertinent to HTI (horizontal transverse isotropy) from VTI (vertical transverse isotropy) is to leave the stiffness matrix c_{ij} alone, and simply reinterpret the meaning of the Cartesian indices i, j. For VTI media, one typical choice is $x_3 = z$, where $\hat{z}$ is the vertical direction at the surface of the earth, or more often the direction down into the earth. Then, the angle of incidence θ is measured with respect to $\hat{z}$, where $\theta = 0$ means parallel to $\hat{z}$ and pointing into the earth, and $\theta = \pi/2$ means horizontal incidence.

Considering aligned vertical fractures, with their axes of symmetry in the direction $x \equiv x_3$, the matrix c_{ij} itself presented in the main text need not change, but the meaning of the angles does change. Clearly, the simplest case to study — and the only one analyzed here — is the case of waves propagating at some angle to vertical but always having a component in the direction $x_3 = x$, while also having $x_2 = y = 0$, thus lying in the xz-plane perpendicular to the fracture plane. (This case is special, but all other wave speeds at other angles of propagation are easily found as a linear combination — depending specifically on the azimuthal angle ϕ at the earth surface — of these values and those in the plane of the fractures themselves.) Then,

$$\theta^H + \theta^V = \frac{\pi}{2}, \tag{B-1}$$

where θ^V corresponds exactly to the θ appearing in all the formulas up to equation 39 in the main text, and θ^H is the effective angle in the xz-plane of incidence under consideration, *i.e.*, the one perpendicular to the vertical fractures in the reservoir. To obtain wave speeds at the angle θ^H, just substitute $\theta \equiv \theta^V = \frac{\pi}{2} - \theta^H$, or write the speeds as

$$^H v_p^2(\theta^H) \equiv v_p^2(\theta^V) = v_p^2(\frac{\pi}{2} - \theta^H), \tag{B-2}$$

$$^H v_{sv}^2(\theta^H) \equiv v_{sv}^2(\theta^V) = v_p^2(\frac{\pi}{2} - \theta^H), \tag{B-3}$$

and

$$^H v_{sh}^2(\theta^H) \equiv v_{sh}^2(\theta^V) = v_p^2(\frac{\pi}{2} - \theta^H). \tag{B-4}$$

Since all the angular dependence in the exact formulas is in the form of $\sin^2\theta$ and $\cos^2\theta$, and since $\sin^2(\frac{\pi}{2} - \theta) = \cos^2\theta$ and vice versa, the entire procedure amounts to switching the locations of $\sin^2\theta$ and $\cos^2\theta$ with $\cos^2\theta^H$ and $\sin^2\theta^H$ everywhere in the exact expressions.

This procedure is obviously very straightforward to implement. The final results analogous to Thomsen's formulas are:

$$^H v_p(\theta^H)/^H v_p(0) \simeq 1 - \frac{\epsilon}{1+2\epsilon}\sin^2\theta^H - \frac{\epsilon-\delta}{1+2\epsilon}\frac{2\cos^2\theta_m^H \sin^2\theta^H \cos^2\theta^H}{[1-\cos 2\theta^H \cos 2\theta_m^H]}, \tag{B-5}$$

$$^H v_{sv}(\theta^H)/^H v_{sv}(0) \simeq 1 + [c_{33}/c_{44}]\,(\epsilon-\delta)\frac{2\cos^2\theta_m^H \sin^2\theta^H \cos^2\theta^H}{[1-\cos 2\theta^H \cos 2\theta_m^H]}. \tag{B-6}$$

and

$$ {}^{H}v_{sh}(\theta^H)/{}^{H}v_{sh}(0) \simeq 1 - \frac{\gamma}{1+2\gamma}\sin^2\theta^H. \tag{B-7} $$

And the $\theta^H = 0$ velocities are: ${}^{H}v_p(0) = \sqrt{c_{11}/\rho} = \sqrt{c_{33}(1+2\epsilon)/\rho}$, ${}^{H}v_{sv}(0) \equiv \sqrt{c_{44}/\rho} = v_s(0)$, and ${}^{H}v_{sh}(0) \equiv \sqrt{c_{66}/\rho} = \sqrt{c_{44}(1+2\gamma)/\rho}$. Also, recall that $\cos^2\theta^H_m = \sin^2\theta^V_m$.

For azimuthal angles $\phi \neq \pm\frac{\pi}{2}$, the algorithm for computing the wave speeds is to replace $\sin^2\theta^V$ by $\cos^2\theta^H\sin^2\phi$ and $\cos^2\theta^V = 1 - \sin^2\theta^V$ by $1 - \cos^2\theta^H\sin^2\phi$ in the exact formulas, and corresponding replacements in the approximate ones. Then, there is no angular dependence when $\phi = 0$ or π as our point of view then lies within the plane of the fracture itself. And, when $\phi = \pm\frac{\pi}{2}$, the above stated results for the xz-plane hold.

Wave equation reciprocity guarantees that the polarizations of the various waves are of the same types as our mental translation from VTI media to HTI media is made.

It is also worth pointing out that the labels SH and SV for the shear waves — although analogous — are, however, surely not strictly valid for the HTI case. For VTI media, the quasi-SH-wave really does have horizontal polarization at least at $\theta = 0$ and $\pi/2$, whereas the corresponding wave for HTI media, instead has polarization parallel ($\|$) to the fracture plane. For VTI media, the so-called quasi-SV-wave has its polarization in the plane of propagation, but this polarization direction is only truly vertical for $\theta = \pm\frac{\pi}{2}$, at which point its polarization is both vertical and perpendicular to the horizontal plane of symmetry. The corresponding situation for HTI media has the wave corresponding to the SV-wave with polarization again in the plane of propagation, but this is actually only vertical at $\theta^H = \frac{\pi}{2}$, and also parallel to the fracture plane; however, for all other angles its polarization has a component that is perpendicular ($\perp$) to the plane of the fractures. So a much more physically accurate naming convention for these waves would make use of the following designations:

$$ {}^{H}v_{sh}(\theta^H) \rightarrow^{H} v_{s\|}(\theta^H), \tag{B-8} $$

for the HTI wave corresponding to the quasi-SH-wave in the VTI case, and

$$ {}^{H}v_{sv}(\theta^H) \rightarrow^{H} v_{s\perp}(\theta^H), \tag{B-9} $$

for the HTI wave corresponding to the quasi-SV-wave in the VTI case. Although this notation is hereby being recommended, it will actually not be used in the main text as the current choices (as well as the various caveats) will no doubt be sufficiently familiar to most readers that it is probably not be essential to make this change in the present paper. In closing, also note that Thomsen (2002) uses the same $\|$ and $\perp$ notation for very similar purposes.

REFERENCES

Backus, G. E., 1962, Long-wave elastic anisotropy produced by horizontal layering: *Journal of Geophysical Research*, **67**, 4427–4440.

Berryman, J. G., 1979, Long-wave elastic anisotropy in transversely isotropic media: *Geophysics*, **44**, 896–917.

Berryman, J. G., and V. Grechka, 2006, Random polycrystals of grains containing cracks: Model of quasistatic elastic behavior for fractured systems: *Journal of Applied Physics*, **100**, 113527.

Dellinger, J., F. Muir, and M. Karrenbach, 1993, Anelliptic approximations for TI media: *Journal of Seismic Exploration*, **2**, 23–40.

Fomel, S., 2004, On anelliptic approximations for qP velocities in VTI media: *Geophysical Prospecting*, **52**, 247–259.

Fowler, P. J., 2003, Practical VTI approximations: A systematic anatomy: *Journal of Applied Geophysics*, **54**, 347–367.

Grechka, V., and M. Kachanov, 2006a, Effective elasticity of fractured rocks: *The Leading Edge*, **25**, 152–155.

Grechka, V., and M. Kachanov, 2006b, Effective elasticity of rocks with closely spaced and intersecting cracks: *Geophysics*, **71**, D85–D91.

Kachanov, M., 1980, Continuum model of medium with cracks: *ASCE Journal of Engineering Mechanics*, **106**, 1039–1051.

Mensch, T., and P. Rasolofosaon, 1997, Elastic-wave velocities in anisotropic media of arbitrary symmetry-generalization of Thomsen's parameters ϵ, δ, and γ: *Geophysical Journal International*, **128**, 43–64.

Musgrave, M. J. P., 1954, On the propagation of elastic waves in aeolotropic media: *Proceedings of the Royal Society of London*, **A226**, 339–366.

Musgrave, M. J. P., 1959, The propagation of elastic waves in crystals and other anisotropic media: *Reports on Progress in Physics*, **22**, 74–96.

Musgrave, M. J. P., 2003, *Crystal Acoustics*: Acoustical Society of America, Leetsdale, Pennsylvania, Chapter 8.

Pederson, Ø., B. Ursin, and A. Stovas, 2007, Wide-angle phase-slowness approximations: *Geophysics*, **72**, S177–S185.

Postma, G. W., 1955, Wave propagation in a stratified medium: *Geophysics*, **20**, 780–806.

Rüger, A., 2002, *Reflection Coefficients and Azimuthal AVO Analysis in Anisotropic Media*: Geophysical Monographs Series, Number 10, SEG, Tulsa, OK.

Sayers, C. M., and M. Kachanov, 1991, A simple technique for finding effective elastic constants of cracked solids for arbitrary crack orientation statistics. *International Journal of Solids and Structures*, **27**, 671–680.

Schoenberg, M., and K. Helbig, 1997, Orthorhombic media: Modeling elastic wave behavior in a vertically fractured earth: *Geophysics*, **62**, 1954–1974.

Thomsen, L., 1986, Weak elastic anisotropy: *Geophysics*, **51**, 1954–1966.

Thomsen, L., 2002, *Understanding Seismic Anisotropy in Exploration and Exploitation*: 2002 Distinguished Instructor Short Course, Number 5, SEG, Tulsa, OK.

Tsvankin, I., 1997, Anisotropic parameters and P-wave velocity for orthorhombic media: *Geophysics*, **62**, 1292–1309.

Tsvankin, I., 2005, *Seismic Signatures and Analysis of Reflection Data in Anisotropic Media*: Handbook of Geophysical Exploration, Seismic Exploration, Volume 29, Elsevier, Amsterdam.

Zhu, T., S. H. Gray, and D. Wang, 2005, Kinematic and dynamic ray tracing in anisotropic media: Theory and application: 75th Annual International Meeting, SEG, Expanded Abstracts, 386–389.

Zhu, T., S. H. Gray, and D. Wang, 2007, Prestack Gaussian-beam depth migration in anisotropic media: *Geophysics*, **72**, S133–S138.

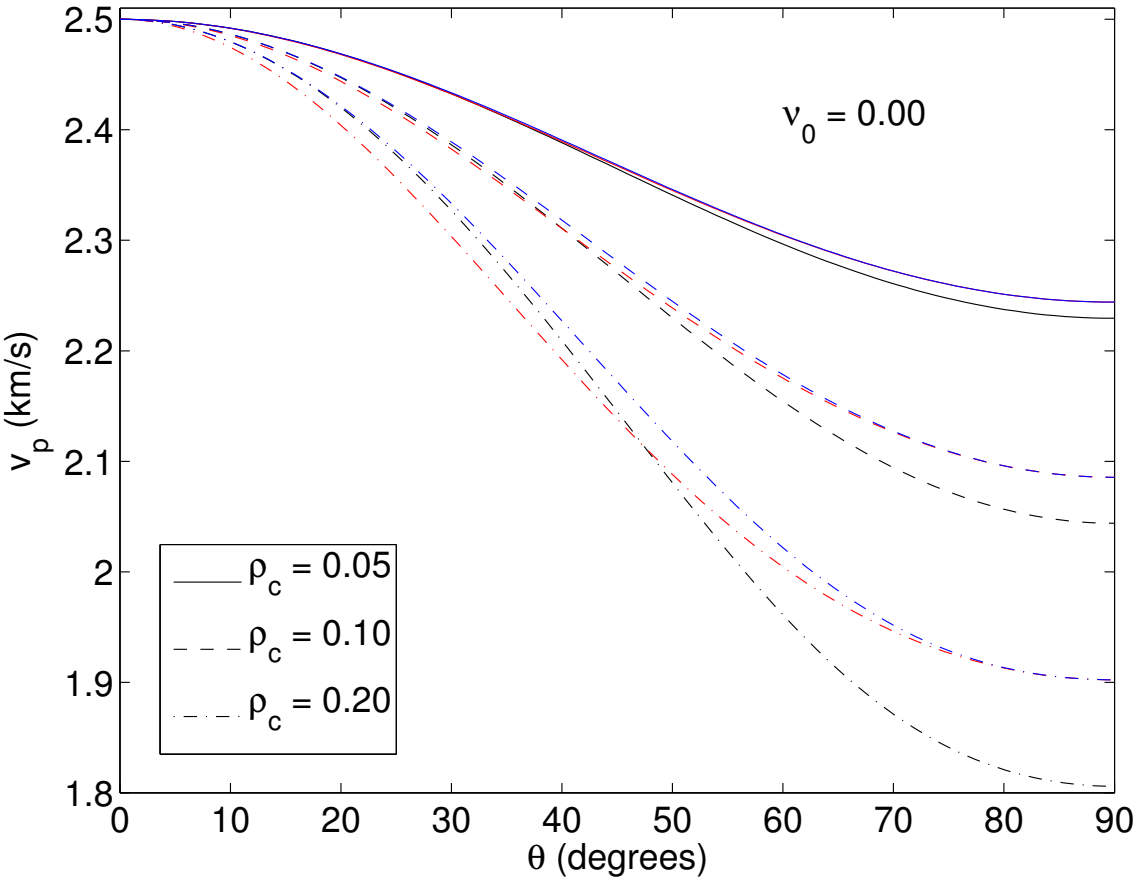

Figure 1: For randomly aligned vertical fractures and VTI symmetry: examples of anisotropic quasi-P compressional wave speed (v_p) for Poisson's ratio of the host medium $\nu_0 = 0.00$. Velocity curves in black are exact for the fracture model discussed in the text. The Thomsen weak anisotropy velocity curves for the same fracture model are then overlain in red. Finally, the new curves for the extended Thomsen approximation valid for stronger anisotropies are overlain in blue. If any of these curves is not visible, it is because one or possibly two other curves are covering them.

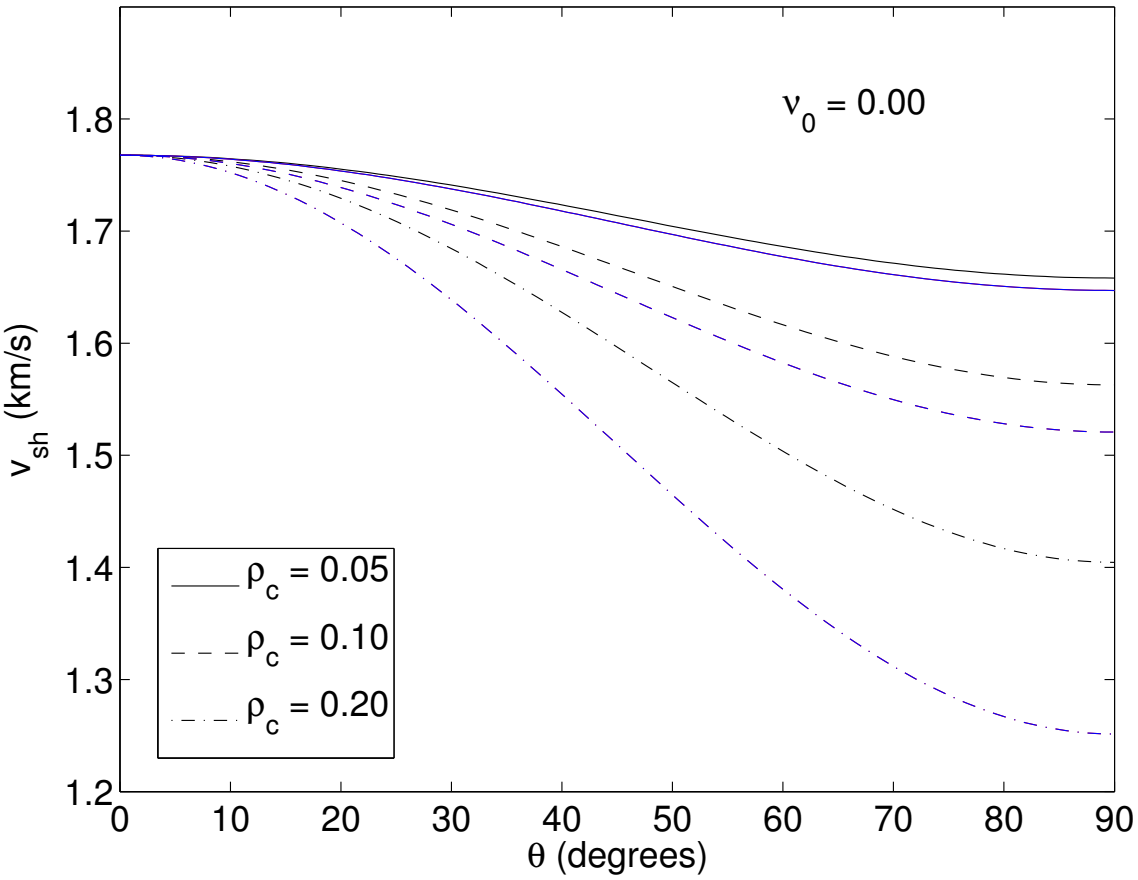

Figure 2: Same as Figure 1 for SH shear wave speed (v_{sh}).

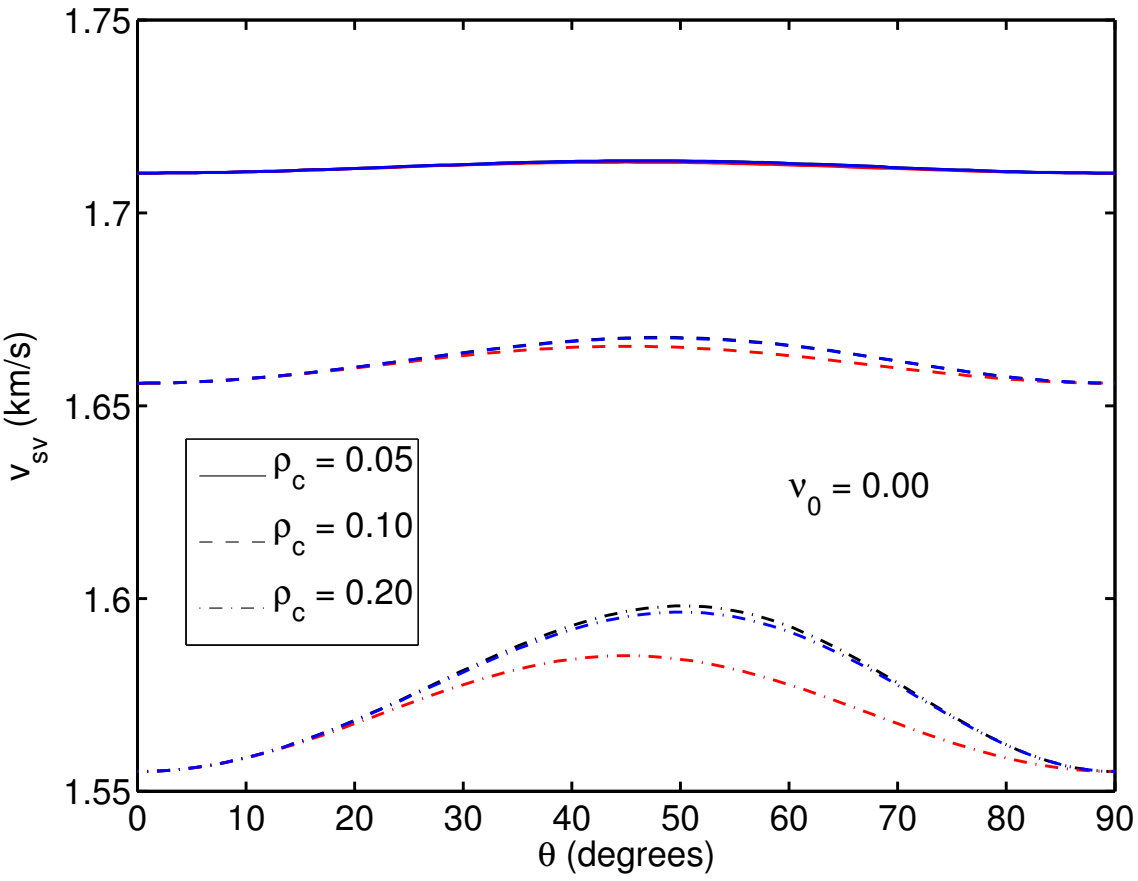

Figure 3: Same as Figure 1 for quasi-SV shear wave speed (v_{sv}).

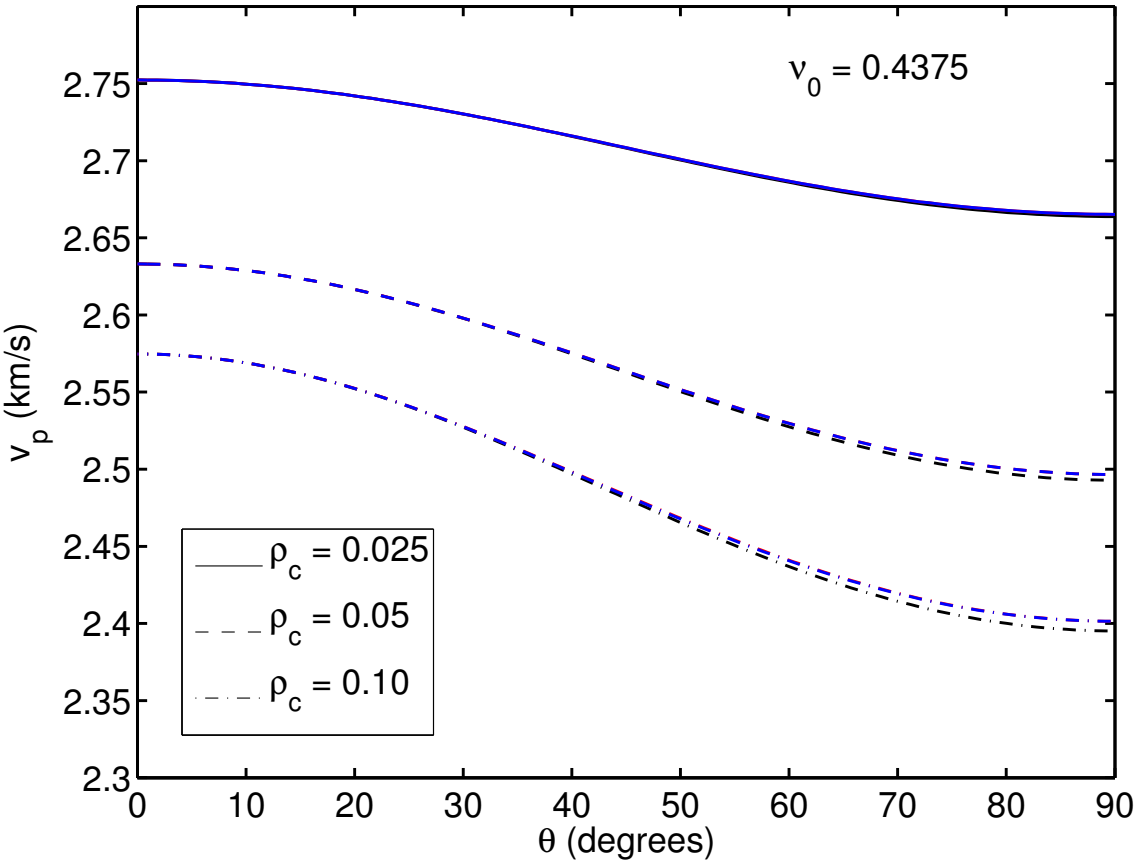

Figure 4: Same as Figure 1, for a different background medium having Poisson's ratio $\nu_0 = 0.4375$.

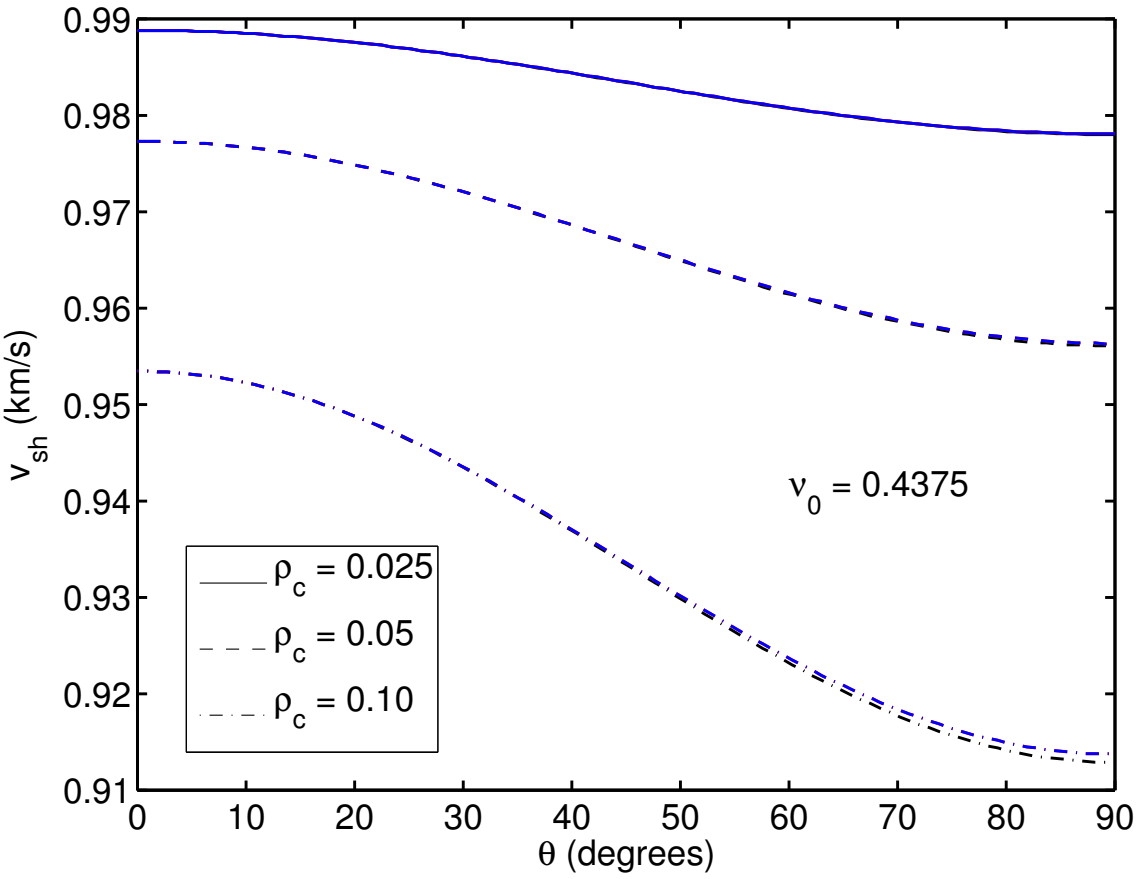

Figure 5: Same as Figure 2, but the value of $\nu_0 = 0.4375$.

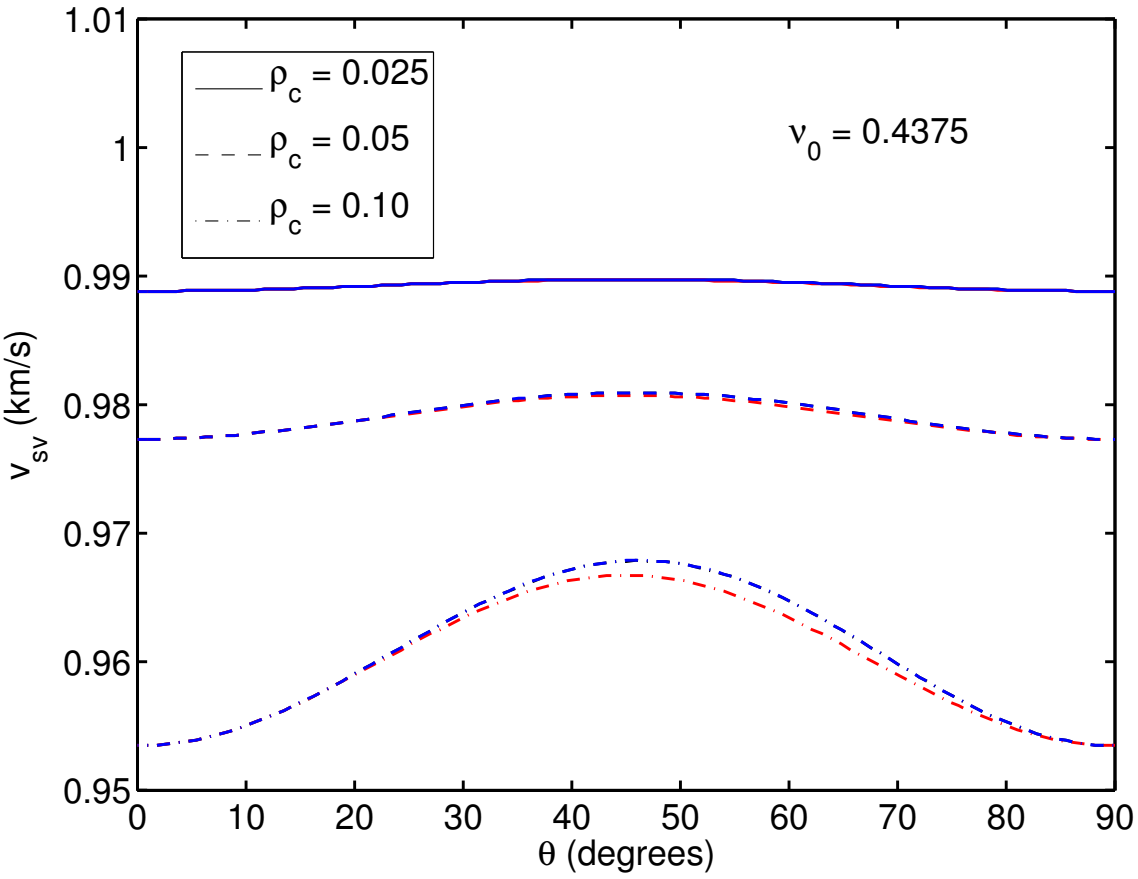

Figure 6: Same as Figure 3, but the value of $\nu_0 = 0.4375$.

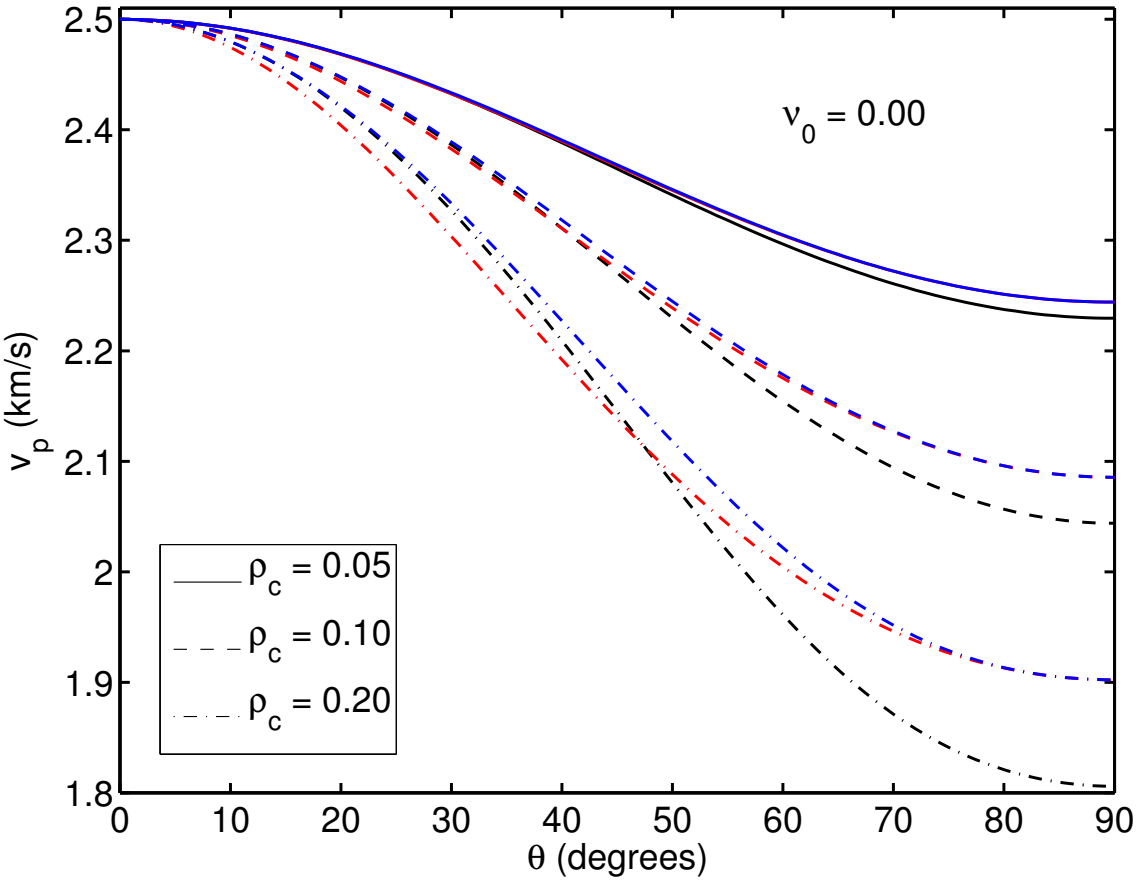

Figure 7: For aligned vertical fractures and HTI symmetry: examples of anisotropic quasi-P compressional wave speed (v_p) for Poisson's ratio of the host medium $\nu_0 = 0.00$. Velocity curves in black are exact for the fracture model discussed in the text. The Thomsen weak anisotropy velocity curves for the same fracture model are then overlain in red. Finally, the new curves for the extended Thomsen approximation valid for stronger anisotropies are overlain in blue. If any of these curves is not visible, it is because one or possibly two other curves are covering them.

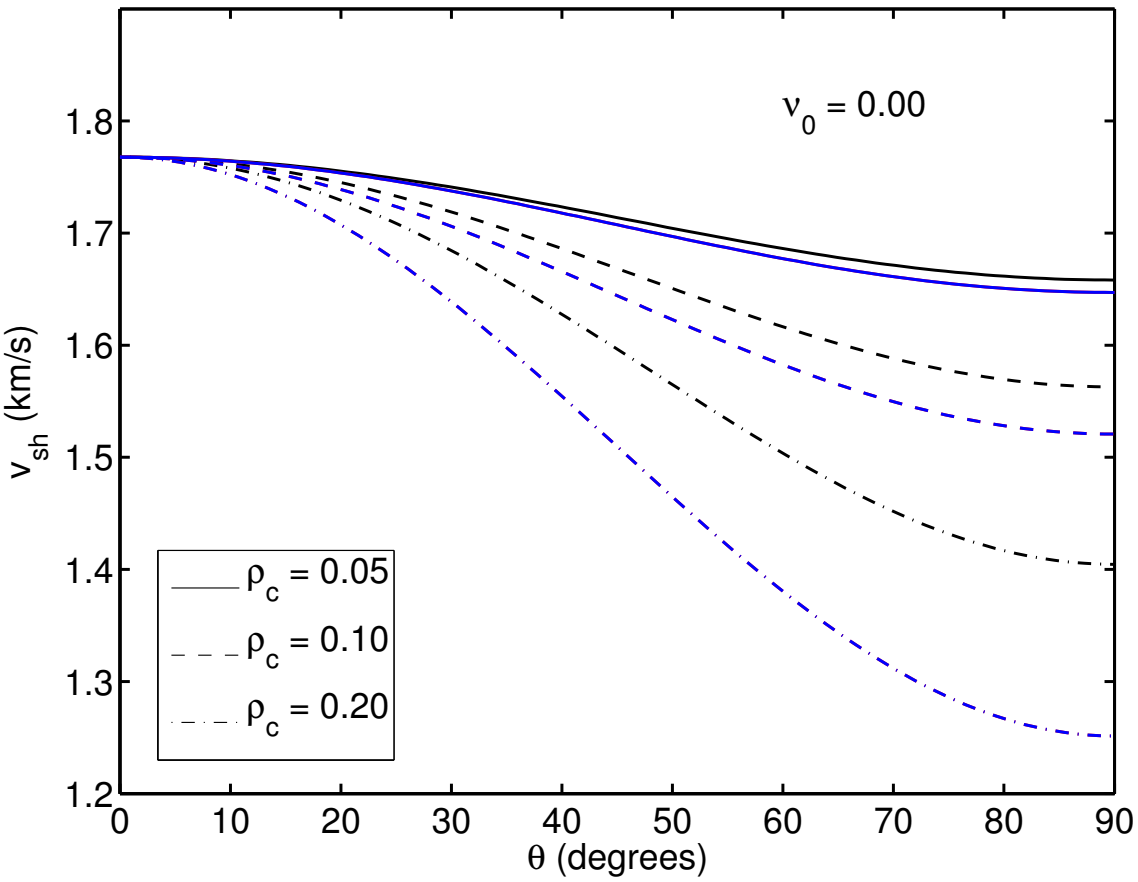

Figure 8: Same as Figure 7 for SH shear wave speed (v_{sh}).

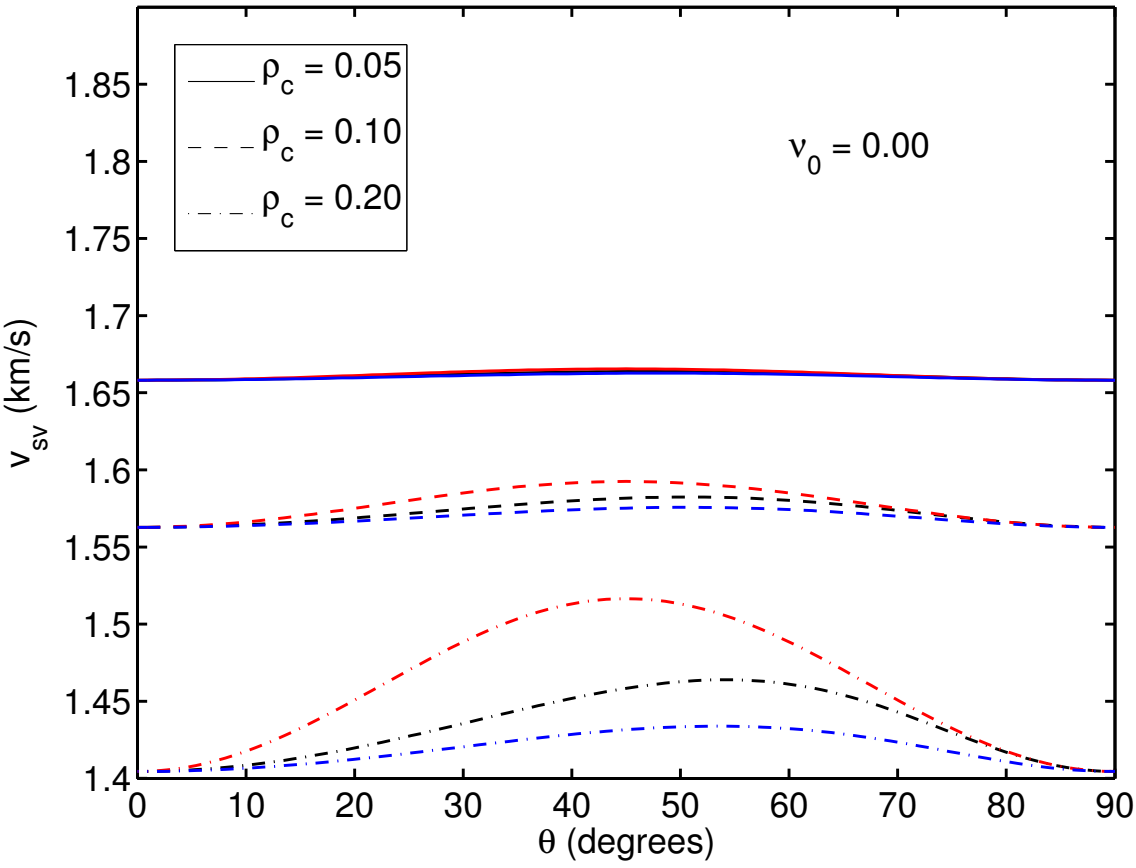

Figure 9: Same as Figure 7 for quasi-SV shear wave speed (v_{sv}).

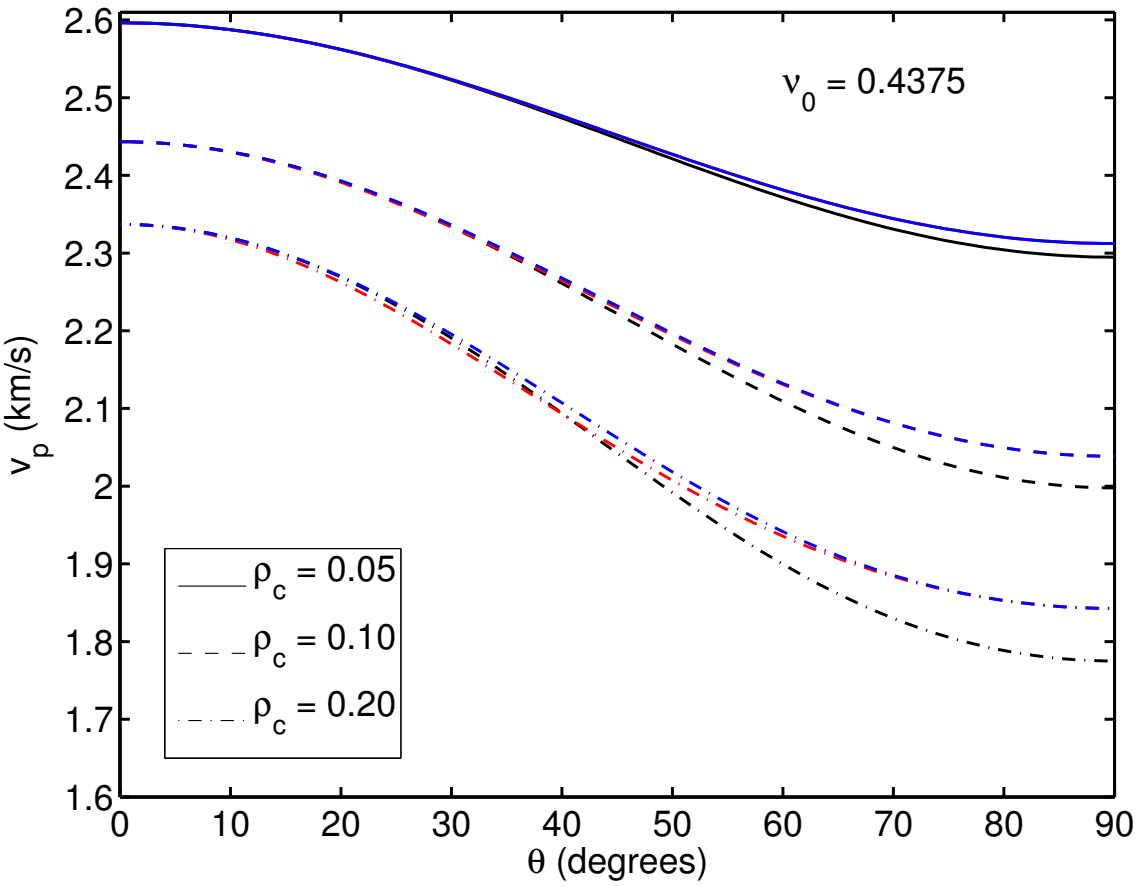

Figure 10: Same as Figure 7, for a different background medium having Poisson's ratio $\nu_0 = 0.4375$.

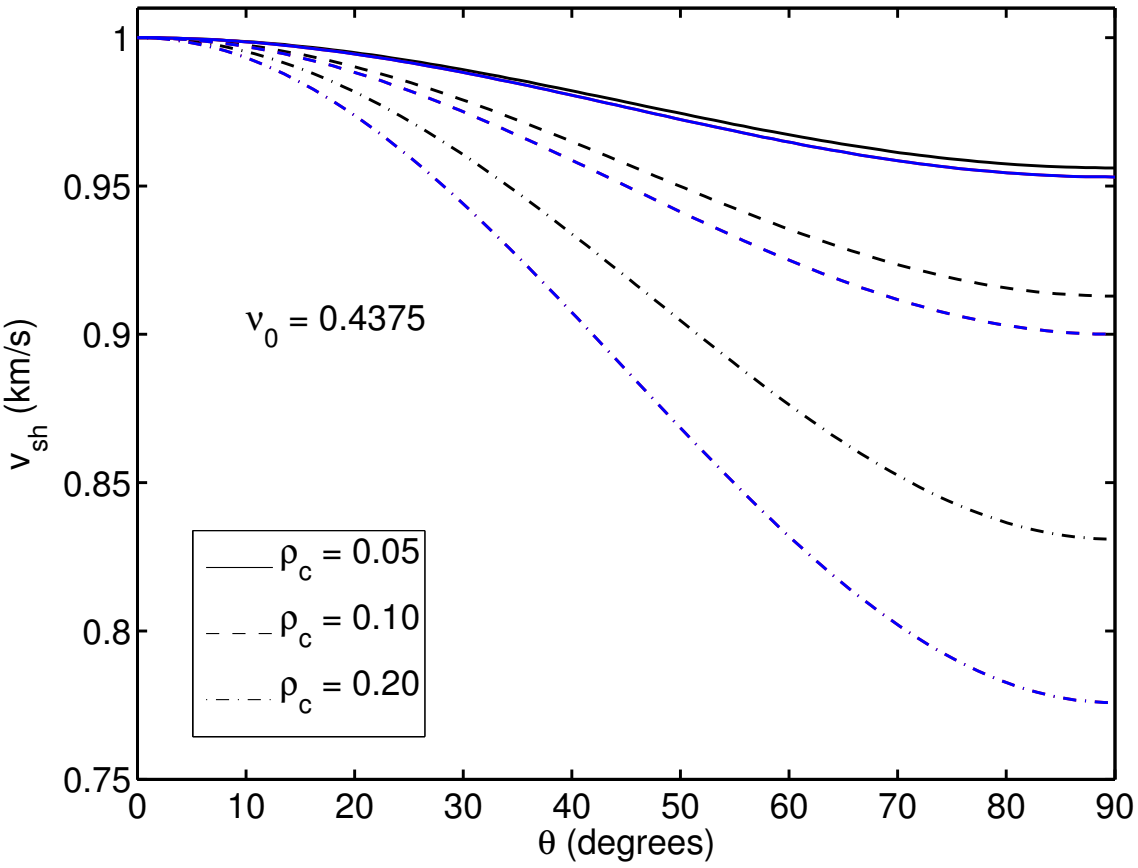

Figure 11: Same as Figure 8, but the value of $\nu_0 = 0.4375$.

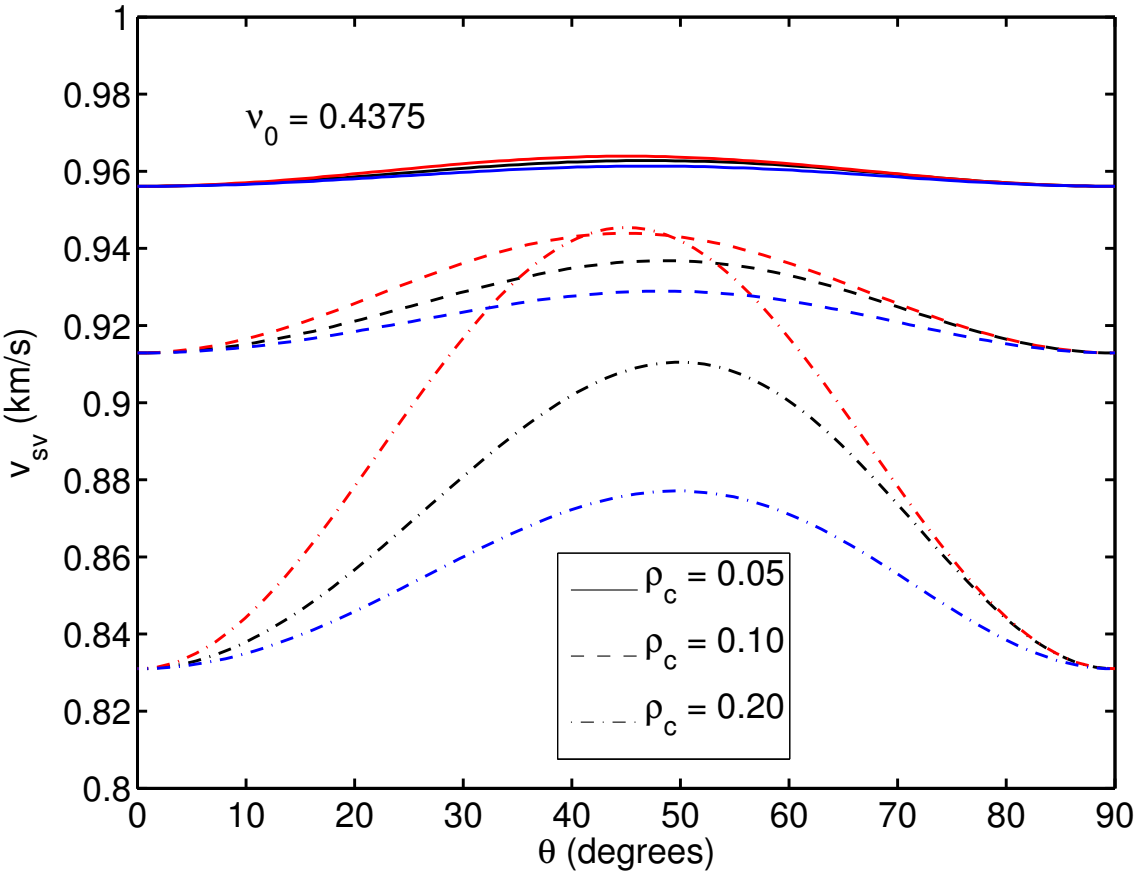

Figure 12: Same as Figure 9, but the value of $\nu_0 = 0.4375$.